water

MDPI

Article

Adapting to Climate Change with Machine Learning: The Robustness of Downscaled Precipitation in Local Impact Analysis

Santiago Mendoza Paz [1,2], Mauricio F. Villazón Gómez [1,*] and Patrick Willems [2,*]

[1] Hydraulic Laboratory, Department of Civil Engineering, Universidad Mayor de San Simón, Cochabamba, Bolivia; santiago.mendoza@ciudadaniabolivia.org
[2] Hydraulics and Geotechnics Section, Department of Civil Engineering, KU Leuven, 3001 Leuven, Belgium
* Correspondence: mauricio.villazon@fcyt.umss.edu.bo (M.F.V.G.); patrick.willems@kuleuven.be (P.W.)

Abstract: The skill, assumptions, and uncertainty of machine learning techniques (MLTs) for downscaling global climate model's precipitation to the local level in Bolivia were assessed. For that, an ensemble of 20 global climate models (GCMs) from CMIP6, with random forest (RF) and support vector machine (SVM) techniques, was used on four zones (highlands, Andean slopes, Amazon lowlands, and Chaco lowlands). The downscaled series' skill was evaluated in terms of relative errors. The uncertainty was analyzed through variance decomposition. In most cases, MLTs' skill was adequate, with relative errors less than 50%. Moreover, RF tended to outperform SVM. Robust (weak) stationary (perfect prognosis) assumptions were found in the highlands and Andean slopes. The weakness was attributed to topographical complexity. The downscaling methods were shown to be the dominant source of uncertainties. This analysis allowed the derivation of robust future projections, showing higher annual rainfall, shorter dry spell duration, and more frequent but less intense high rainfall events in the highlands. Apart from the dry spell's duration, a similar pattern was found for the Andean slopes. A decrease in annual rainfall was projected in the Amazon lowlands and an increase in the Chaco lowlands.

Keywords: climate change; precipitation; statistical downscaling; machine learning; uncertainty; the Andes

check for updates

Citation: Mendoza Paz, S.; Villazón Gómez, M.F.; Willems, P. Adapting to Climate Change with Machine Learning: The Robustness of Downscaled Precipitation in Local Impact Analysis. *Water* **2024**, *16*, 3070. https://doi.org/10.3390/w16213070

Academic Editors: María Jesús Esteban Parra, Sonia Raquel Gámiz-Fortis and Matilde García-Valdecasas Ojeda

Received: 20 September 2024
Revised: 19 October 2024
Accepted: 23 October 2024
Published: 26 October 2024

Copyright: © 2024 by the authors. Licensee MDPI, Basel, Switzerland. This article is an open access article distributed under the terms and conditions of the Creative Commons Attribution (CC BY) license (https://creativecommons.org/licenses/by/4.0/).

1. Introduction

Climate variability affects human and natural ecosystems, which are believed to be altered by climate change [1]. These changes, especially in climatic extremes, will translate into societal risks. It is widely known that precipitation directly influences drought and flood episodes. The examples of recent disaster events around the world, e.g., the bushfires in Australia caused partially by severe droughts [2] or the mudslides due to high precipitation extremes in Brazil [3], are some of the warnings about our vulnerability as societies regarding climatic extremes.

The focus region of this study, Bolivia, is no exception. Bolivia is a country that depends highly on agriculture. Hence, how climate change will affect droughts is crucial. Moreover, around 66% of the region is prone to flooding [4], and the biggest cities do not have robust infrastructure to cope with flooding episodes. The most recent notorious flood and drought events were in 2002, 2006–2007, 2007–2008, and 2009–2010, with estimated economic consequences of around 1244 million American dollars [4]. In addition, the World Bank [5] noted that Bolivia is highly vulnerable to climate change. In their study, the estimated disaster deficit index (DDI), a ratio of the potential economic loss caused by a natural disaster to the country's economic resilience, was about 1.47. The latter number can be translated into a lack of ability to cope with extremes [6]. In this sense, natural hazards enhanced by climate change would significantly impact ecological systems and

socio-economic sectors. Therefore, investigating the possible changes in flood and drought events at the local level is required.

The primary information to study the impacts of climate change is provided by global climate models, commonly known as GCMs [7,8]. However, an increased resolution is required for studies at the local level. One possibility is to perform statistical downscaling by establishing relationships between the large-scale climate and local observations. Its use has many advantages, for instance, low computational costs and large climate model ensembles. The latter takes importance since considering climate model ensembles is advised to account for the uncertainties [9,10]. However, one has to consider that the statistical downscaling methods (SDMs) contain drawbacks and assumptions that need to be studied before their application for impact studies. These generally depend on the type of SDM used. In the literature, various types of SDMs have been tested, including machine learning methodologies. Machine learning is known for its good performance on complex non-linear problems, and it has been proven that they can work within the climate change context [11–16] and in studying extremes for satellite estimates [17,18]. However, most machine learning applications are oriented toward weather forecasting, and it remains unclear if they can be used for assessing extremes in the climate change context.

The problem is that the architectures cannot be calibrated directly for GCMs; hence, they must be calibrated between observations (local scale) and re-analysis (large scale). Then, a bias correction is performed by comparing GCMs and re-analysis to apply the derived architecture to the GCMs. This represents a drawback: the prior correction of the GCMs will enlarge the uncertainties due to the addition of another step in the cascade [19]. There are some ways to bridge the gap, for instance, by constructing a machine learning methodology that performs an advanced bias correction technique. In this sense, one can avoid enlarging the cascade of uncertainties since the advance bias correction will function as a downscaling technique.

Moreover, no matter how the methodologies are built, they have two important assumptions: the statistical relationships are invariant in time and under different forcing conditions. These are crucial, and many studies have demonstrated violations of these assumptions. For instance, violations of the stationary assumptions by implementing a perfect model experimental design on empirical statistical downscaling (ESD) methods were found [20]. However, this was demonstrated to depend on the season and geographical location. Vrac et al. [8] used a nonhomogeneous stochastic weather typing (NSWT) method and regional climate models as pseudo-reality to evaluate the stationary assumptions. They found that the relationships were affected by the forcing conditions, i.e., the relationships might not remain invariant under different forcing conditions. In addition to the fact that these assumptions are difficult to investigate as future observations are unavailable, the studies that performed this evaluation using machine learning techniques are rare.

This work aims to evaluate the skill and assumptions of two machine learning techniques, dividing the observations into two large periods. Then, significant changes in impact-related research indicators (RIs) are projected to understand how future climate might shape floods and droughts in the region. RIs representing the climate conditions for floods and drought are used for that. Moreover, four future scenarios from the state-of-the-art GCMs (CMIP6) are analyzed in the projections. The uncertainty share from the SDMs is also investigated to obtain insights on the relative contribution to the total uncertainty in the study.

2. Materials and Methods

2.1. Study Area

Located in the center of South America, Bolivia is a country with large variations in topography. Some regions are as high as 6500 m.a.s.l., contrasted with others at less than 800 m.a.s.l. (Figure 1). It also contains much diversity in ecosystems and landscapes. These factors shape the temperature and precipitation of the different regions in the country. A standard classification of the different zones in the country in terms of altitudes is as

follows [21]: the lowlands (<800 m.a.s.l.), the Andean slopes (between 800 and 3200 m.a.s.l.) and the highlands (between 3200 and 6500 m.a.s.l). Although the climatic conditions can be highly different within each zone, some common characteristics exist.

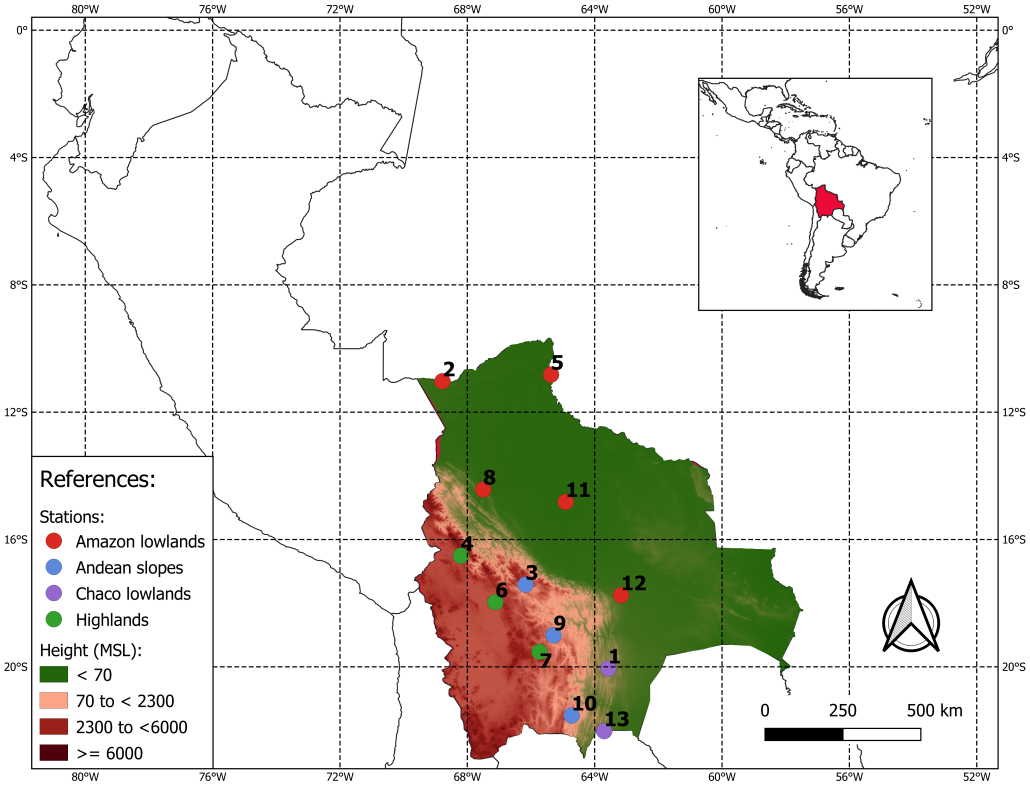

Figure 1. Location of the study area. In red is the geographical position of the precipitation stations (observations) of the Amazon lowlands, in purple the Chaco lowlands, in blue the Andean slopes, and in green the highlands. The graph presents the topography as differences in altitudes above sea level. The numbers represent the ID of the stations (see Table 1).

The lowlands contain high humidity percentages with medium to high temperatures, and the precipitations range from 1000 to 2000 mm per year. Note that this is a generalization as the lowland system is highly complex. For instance, the zone contains two different climates, with some important differences: the Amazon in the north and the Chaco-Pantanal in the south, with tropical and steppe climates, respectively. The Andean slopes represent the zones between the Andean valleys and the transitions from the Andes to the lowlands. The temperatures tend to be moderate, and the precipitation varies from low precipitation rates up to more than 2000 mm per year. The highlands are characterized by low temperatures (10 °C mean annual temperature) and perpetual snow in the highest points. The solar radiation is intense but does not increase the temperatures as there is little moisture to carry the energy through the air. The precipitation varies from 200 to 500 mm per year, but the southwest part of the highlands contains precipitation lower than 200 mm per year [22].

This heterogeneity made the analysis of climate change more challenging but also interesting. The different zones required a specific investigation as the analysis in one of the zones might not be valid in the others. Therefore, the SDMs were analyzed in 13 locations in Bolivia (Figure 1). These locations were contained within each zone: (i) the Amazon lowlands were represented with five stations, (ii) the Chaco lowlands had two stations, (iii) the Andean slopes had three stations, and (iv) the highlands had three stations. Table 1 shows the stations and their coordinates. The stations from this work were used to monitor meteorological conditions at the airports of different cities and small towns, making the stations' data highly reliable.

Table 1. Stations used for this analysis.

ID	Name	Lat. [°]	Lon. [°]	Height [MSL]	Zone
1	Camiri	−20.05	−63.57	810	Chaco lowlands
2	Cobija	−11.03	−68.78	235	Amazon lowlands
3	Cochabamba	−17.42	−66.17	2548	Andean slopes
4	El Alto	−16.51	−68.2	4071	Highlands
5	Guayaramerin	−10.82	−65.37	130	Amazon lowlands
6	Oruro	−17.97	−67.12	3702	Highlands
7	Potosí	−19.53	−65.73	4100	Highlands
8	Rurrenabaque	−14.43	−67.5	204	Amazon lowlands
9	Sucre	−19.01	−65.29	2904	Andean slopes
10	Tarija	−21.53	−64.72	1875	Andean slopes
11	Trinidad	−14.82	−64.91	156	Amazon lowlands
12	Trompillo	−17.75	−63.17	413	Amazon lowlands
13	Yacuiba	−22.02	−63.7	580	Chaco lowlands

2.2. Observed Series and Re-Analysis

This work used 13 stations representing each zone (Amazon lowlands, Chaco lowlands, Andean slopes, and highlands). The stations belonged to the Bolivian national service of meteorology and hydrology (SENAMHI). Moreover, these were summaries of the data from nearby airports monitoring meteorological conditions. Two periods were used: (i) 1981–2010 for calibration of the downscaling methods and (ii) 1961–1980 for validating the methodologies in terms of relative error and the analysis of their assumptions.

The re-analysis datasets used in this study were the latest product of the European Centre for Medium-Range Weather Forecasts (ECMWF). This version (ERA5) replaces the previously widely known ERA-Interim. The 30-year period of 1981–2010 was used to calibrate the relationships. The re-analysis dataset contained 26 variables at different pressure levels. However, only the most correlated variables were used: total precipitation, specific humidity at 500 hPa, 850 hPa, and 1000 hPa. The correlation matrices for each station's precipitation and the 26 variables (at 500, 850, and 1000 hPa) of ERA5 are presented in the Supplementary Materials. The calibration of the relationships with a re-analysis to later use them on bias-corrected GCMs is common in statistical downscaling studies that use perfect prognosis methodologies [23].

2.3. Global Climate Models

An ensemble of 20 global climate models from the CMIP6 era was used. The variables were precipitation and specific humidity at 500 hPa, 850 hPa, and 1000 hPa. These variables were chosen since they contained the highest correlation with the study area stations and were the same variables used in the re-analysis dataset. The correlation matrices for each station are presented in the Supplementary Materials. Table 2 presents the climate models used in this study.

Table 2. Global climate models and simulations used in this work.

Nr.	Model	Resolution *	Historical	SSP1-2.6	SSP2-4.5	SSP3-7.0	SSP5-8.5	Variant Label
1	ACCESS-CM2	1.9 × 1.3	1	1	1	1	1	r1i1p1f1
2	ACCESS-ESM1-5	1.9 × 1.3	1	1	1	1	1	r1i1p1f1
3	CanESM5	2.8 × 2.8	25	1	1	1	1	r1i1p1f1-r25i1p1f1
4	CESM2-WACCM	1.3 × 0.9	1	1	1	1	1	r1i1p1f1
5	CMCC-CM2-SR5	1 × 1	1	1	1	1	1	r1i1p1f1
6	EC-Earth3	0.7 × 0.7	1	1	1	1	1	r1i1p1f1
7	EC-Earth3-Veg	0.7 × 0.7	1	1	1	1	1	r1i1p1f1
8	EC-Earth3-Veg-LR	1.1 × 1.1	1	1	1	1	1	r1i1p1f1
9	FGOALS-g3	2 × 2	1	1	1	1	1	r1i1p1f1

Table 2. *Cont.*

Nr.	Model	Resolution *	Historical	SSP1-2.6	SSP2-4.5	SSP3-7.0	SSP5-8.5	Variant Label
10	IITM-ESM	1.9 × 1.9	1	1	1	1	1	r1i1p1f1
11	INM-CM4-8	2 × 1.5	1	1	1	1	1	r1i1p1f1
12	INM-CM5-0	2 × 1.5	1	1	1	1	1	r1i1p1f1
13	IPSL-CM6A-LR	2.5 × 1.3	1	1	1	1	1	r1i1p1f1
14	KACE-1-0-G	1.9 × 1.3	1	1	1	1	1	r1i1p1f1
15	MIROC6	1.4 × 1.4	1	1	1	1	1	r1i1p1f1
16	MPI-ESM1-2-HR	0.9 × 0.9	1	1	1	1	1	r1i1p1f1
17	MPI-ESM1-2-LR	1.9 × 1.9	1	1	1	1	1	r1i1p1f1
18	MRI-ESM2-0	1.1 × 1.1	1	1	1	1	1	r1i1p1f1
19	NorESM2-LM	2.5 × 1.9	1	1	1	1	1	r1i1p1f1
20	NorESM2-MM	1.3 × 0.9	1	1	1	1	1	r1i1p1f1
	Total number of runs		44	20	20	20	20	

Note: * The resolution is in Lon [°] × Lat [°] format.

2.4. Research Indicators

This work used the Expert Team on Climate Change Detection and Indices (ETCCDI) indices, regarded here as research indicators (RIs), to address the analysis of the methodologies and the associated Climate Change Signal (CCS). According to the World Meteorological Organization (WMO) and the IPCC Assessment reports, these indices are commonly applied in the community. Not all the indices were used, but the ones suitable for an impact analysis on hydrological extremes. More precisely, the RIs considered were the summer precipitation (R1), the spring precipitation (R2), the autumn precipitation (R3), the winter precipitation (R4), the maximum duration of dry spells (R5), the annual precipitation (R6), the maximum daily precipitation of a 30-year return period (R7), the maximum daily precipitation of a 10-year return period (R8), the annual number of days with precipitation greater than 10 mm (R9), the annual number of days with precipitation greater than 20 mm (R10), and the annual number of days with precipitation greater than 30 mm (R11). Note that R1, R2, R3, R4, and R6 denote only precipitation accumulation; however, they are important for drought analysis, especially R6. By including this set of impact-related indicators, one can have an idea about the local impacts of climate change on the hydrological extremes. Table 3 presents a summary of these indices and some important characteristics.

Table 3. Research indicators used in this study and their link to hydrological extremes.

Name	Description	Units	Link
R1	Summer precipitation	mm/season	Droughts
R2	Spring precipitation	mm/season	Droughts
R3	Autumn precipitation	mm/season	Droughts
R4	Winter precipitation	mm/season	Droughts
R5	Maximum duration of dry spells	days	Droughts
R6	Annual precipitation	mm/year	Droughts
R7	Maximum daily precipitation of a 30-year return period	mm/day	Floods
R8	Maximum daily precipitation of a 10-year return period	mm/day	Floods
R9	Annual count of days with precipitation greater than 10 mm	-	Floods
R10	Annual count of days with precipitation greater than 20 mm	-	Floods
R11	Annual count of days with precipitation greater than 30 mm	-	Floods

2.5. Machine Learning Techniques

Two machine learning methodologies were chosen to perform statistical downscaling: random forest and support vector machine. This work refers to the random forest and support vector machine as SD-ML-4 and SD-ML-5, respectively. The main reason for inves-

tigating machine learning rather than more conventional techniques is the high capacity of the methodologies to learn non-linear relationships, a key feature when downscaling precipitation from GCMs. The characteristics of each methodology are presented in this section. Moreover, some general features of the architectures considered for this work and the motivation of the choice are presented.

2.5.1. Random Forest (SD-ML-4)

The use of tree ensemble methods in statistical downscaling is interesting as the choice of the best model or architecture is not "pre-defined"; instead, many well-estimated (data-driven) architectures are built from random samples of the data, and later, the average of all these estimations is regarded as the model architecture. The method proposed by Breiman [24], called random forest, was adopted in this work. The reason for the choice of this specific method among the other "tree ensemble methods" (e.g., Adaboost) is that the methodology is less demanding in computer resources, and at the same time, it helps in determining (data-driven) the important variables for the regression [17]. To build the architecture of the method, the python library "Scikit-learn" [25] was used.

The balance between model complexity and regularization in random forest architectures can be controlled by adjusting five hyperparameters [26]: (i) the number of trees in the forest ($N_{estimators}$), (ii) the maximum depth or levels of each tree (Max_{depth}), (iii) the minimum number of data points required to split an internal node ($Min_{samples_{split}}$), (iv) the minimum number of data points required to be a leaf node ($Min_{samples_{leaf}}$), and (v) the maximum number of features considered for the best split in the node ($Max_{features}$). The optimal combination of the parameters was determined with GridSearchCV from the sklearn python library. However, Max_{depth} was left out since a sensitivity analysis was carried out to determine that parameter. A trial-and-error procedure was performed, varying Max_{depth} from 1 to 50. The outcome of this analysis can be found in the Supplementary Materials.

It is important to note that the methodology is designed to converge (in terms of error optimization) with the increase in the number of trees [24]. Hence, the more trees are defined (larger $N_{estimators}$ value), the better the model. The only problem with increasing the number of trees is computational time [17]. With all the parameters as default, the change in accuracy from 1 to 500 trees was checked. It was observed that after 100, increasing the number to a larger value increased computational time without improving accuracy. Therefore, the range of $N_{estimators}$ was limited to 100.

2.5.2. Support Vector Machines (SD-ML-5)

The implementation of this method follows the spirit of quantile mapping parametric approaches but with a modification in the derivation of the transformation functions. Instead of assuming a specific transformation to correct the precipitation quantiles of the coarse scale (global climate models) to the local scale (observations), an architecture with a support vector machine was constructed to derive the most suitable relation to correct the quantiles. This way, a prior assumption on how the transformation function might look was avoided. The R library "kernlab" was used for that purpose [27].

The kernel-based neural networks, formally called support vector machines (SVMs), were developed to overcome the weaknesses of traditional machine learning implementations [15,28], such as the commonly applied artificial neural networks (ANNs). One of the limitations of traditional implementations is that the models tend to find the optimal local solution, not the global one, whereas this limitation is not present in SVMs [28]. Moreover, according to Tripathi et al. [15], SVMs' model architecture is automatically derived, avoiding the subjectivity that is present in more traditional methodologies (e.g., artificial neural networks). The study also mentions that more flexibility is involved since SVMs can use many kernel functions. A kernel function helps to overcome the problem of high dimensionality, i.e., it is a simple way to translate relationships derived in higher dimensions.

There is no consensus on the most suitable kernel for downscaling rainfall; however, previous implementations of this methodology (e.g., [15]) demonstrated that the Gaussian

radial basis kernel worked fine in downscaling studies. Moreover, the Gaussian radial basis is a general-purpose kernel typically used in works without in-depth prior knowledge about the data [27]. The Gaussian radial basis kernel has two important hyperparameters: the kernel's width (sigma) and the cost of the error minimization function (C). Sigma shapes the transfer function, while C helps to prevent a result with local minima in the optimization. A sensitivity analysis was conducted to select the values of the hyperparameters for each station. Different combinations in the range of [0.0001, 0.1] and [1, 120] for sigma and C, respectively, were tested. Then, the results' empirical cumulative distribution function (ECDF) was contrasted with the raw GCM series and the observations. The values that gave the closest ECDF with respect to the observations were chosen as optimal. The sensitivity analysis is presented in the Supplementary Materials.

2.6. Variance Decomposition

The work of Räty et al. [29] suggested that reliable downscaling studies must include the SDMs' uncertainty contribution and many downscaling methods. Following that line, the uncertainty contribution from the downscaling methodologies was quantified by variance decomposition. The uncertainty was calculated with all research indicators and the four future scenarios. Note that the SDMs' uncertainty share results and relative errors had to be combined to analyze the robustness of future projections.

The variance decomposition procedure quantified the different elements and their interactions contributing to the overall uncertainties. For that, the total variance was split into the fractions associated with the GCMs, SSP scenarios and downscaling techniques:

$$var_{(t)} = var_{(g)} + var_{(s)} + var_{(d)} + var_{(gs)} + var_{(gd)} + var_{(sd)} + var_{(gsd)} \quad (1)$$

where $var_{(t)}$ is the total variance, $var_{(g)}$ is the variance associated with the GCM ensemble, $var_{(s)}$ that associated with the different future SSP scenarios, $var_{(d)}$ that associated with the different downscaling methods, and $var_{(gs)}$, $var_{(gd)}$, $var_{(sd)}$, and $var_{(gsd)}$ are associated with the interactions between the three contributors. Note that if the full variability of all the contributors is summed, the actual result is larger than the total variance because each contributor contains interactions. Since the focus of this work was the statistical downscaling methodologies, the total contribution from the different techniques was quantified as:

$$var_{(total,d)} = var_{(d)} + var_{(gd)} + var_{(sd)} + var_{(gsd)} \quad (2)$$

To calculate the terms in Equations (1) and (2), the analysis of variance was applied. The procedure was implemented on all research indicators to analyze the behavior of the uncertainty share under different situations. First, the variance only due to each contributor's variability was obtained:

$$var_{(g)} = \frac{1}{ngcm} SUM_{i=1}^{ngcm} (X_{i..} - X_{...})^2 \quad (3)$$

$$var_{(s)} = \frac{1}{nscen} SUM_{j=1}^{nscen} (X_{.j.} - X_{...})^2 \quad (4)$$

$$var_{(d)} = \frac{1}{nsdm} SUM_{k=1}^{nsdm} (X_{..k} - X_{...})^2 \quad (5)$$

Second, the variance due to the interaction between two contributors was calculated:

$$var_{(gs)} = \frac{1}{ngcm} SUM_{i=1}^{ngcm} \frac{1}{nscen} SUM_{j=1}^{nscen} (X_{ij.} - X_{i..} - X_{.j.} + X_{...})^2 \quad (6)$$

$$var_{(gd)} = \frac{1}{ngcm} SUM_{i=1}^{ngcm} \frac{1}{nsdm} SUM_{k=1}^{nsdm} (X_{i.k} - X_{i..} - X_{..k} + X_{...})^2 \quad (7)$$

$$var_{(sd)} = \frac{1}{nscen} SUM_{j=1}^{nscen} \frac{1}{nsdm} SUM_{k=1}^{nsdm} (X_{.jk} - X_{.j.} - X_{..k} + X_{...})^2 \quad (8)$$

Lastly, the variance due to the interaction between the three contributors was calculated:

$$var_{(gsd)} = \frac{1}{ngcm} SUM_{i=1}^{ngcm} \frac{1}{nscen} SUM_{j=1}^{nscen} \frac{1}{nsdm} SUM_{k=1}^{nsdm} (X_{ijk} - X_{ij.} - X_{i.k} - X_{.jk} + X_{i..} + X_{.j.} + X_{..k} - X_{...})^2 \quad (9)$$

where the dots represent the averages with respect to the indices they are substituting, i represents the GCMs (i models), j represents the SSP scenarios (j scenarios), and k represents the downscaling methods (k methods); $ngcm, nscen$, and $nsdm$ represent the number of GCMs (20), future scenarios (4), and SDMs (2) used in the downscaling study, respectively. For more information about the procedure, the reader is referred to [30–32].

2.7. Significance of the Signal

It is important to study the climate change signal together with its significance. In impact studies, the focus is on how climate might change and how significant that change is. For that, Tabari et al. [33] proposed an interesting approach to compare the derived signal against the natural variability of the climate as seen in global climate models. More specifically, 25 different runs from CanESM5 (r1i1f1p1, r2 i1f1p1, r3 i1f1p1, . . . , r25 i1f1p1) were considered to account for the analysis of natural variability (signal-to-noise ratio, S2NR). The several historical experiments of CanESM5 were regarded as a "historical ensemble". Each run was initialized using different starting conditions (points in the preindustrial historical run). One can assume that the "historical ensemble" represents the model's internal variability. Therefore, one can calculate the research indicators involved in the analysis with all the runs in the historical period and attribute the differences (noise) to the internal variability of the climate system of CanESM5. This noise is considered "natural variability".

In this procedure, the climate change signal ($\overline{CCS_{ensemble}}$), calculated for each relevant statistic, i.e., research indicator (R_n) as R_n^{Proj} divided by R_n^{Obs}, is said to be significant if it is sufficiently large compared to the natural variability (S2NR). For that, the null hypothesis (H_0) of the Z test considers no significant change or that the S2NR is greater than the change, i.e., the mean of CCS is equal to one. Accepting the null hypothesis means that the change is not significant, while rejecting it (accepting the alternative hypothesis H_1) means that the change is significant. The critical value Z from a standard normal distribution corresponding to a significance level of 5% (95% of confidence) was used to test the hypothesis. Hence, if a $|Z| = \left| \frac{\overline{CCS_{ensemble}} - 1}{STDEV_{25runsCanESM5}} \right|$ was greater than 1.96 (critical Z value), the null hypothesis was rejected.

3. Results

3.1. Relative Errors

The results are summarized as follows: (i) the highlands are represented by El Alto, Oruro, and Potosi stations; (ii) the Andean slopes are represented by Cochabamba, Sucre, and Tarija; (iii) the Amazon lowlands are represented by Cobija, Guayaramerin, Rurrenabaque, Trinidad, and Trompillo; and (iv) Camiri and Yacuiba represent the Chaco lowlands. The relative errors (a measure of the skill) were obtained by comparing the observations and the downscaled series research indicators obtained from 1961 to 1980.

3.1.1. The Highlands

Figure 2 shows large relative errors from the GCMs. The SDMs' added value is seen on the three stations, along with the precipitation amount indicators (R1, R2, R3, and R6) as they reduce the coarse-scale relative error, in many cases below 25%. The small added value seen on R4 was probably due to the low precipitation artifacts in the dry season. The winter precipitation in the zone (dry season) was characterized by a strong water deficit (almost no rain). Hence, the corrections of the SDMs might not be too effective.

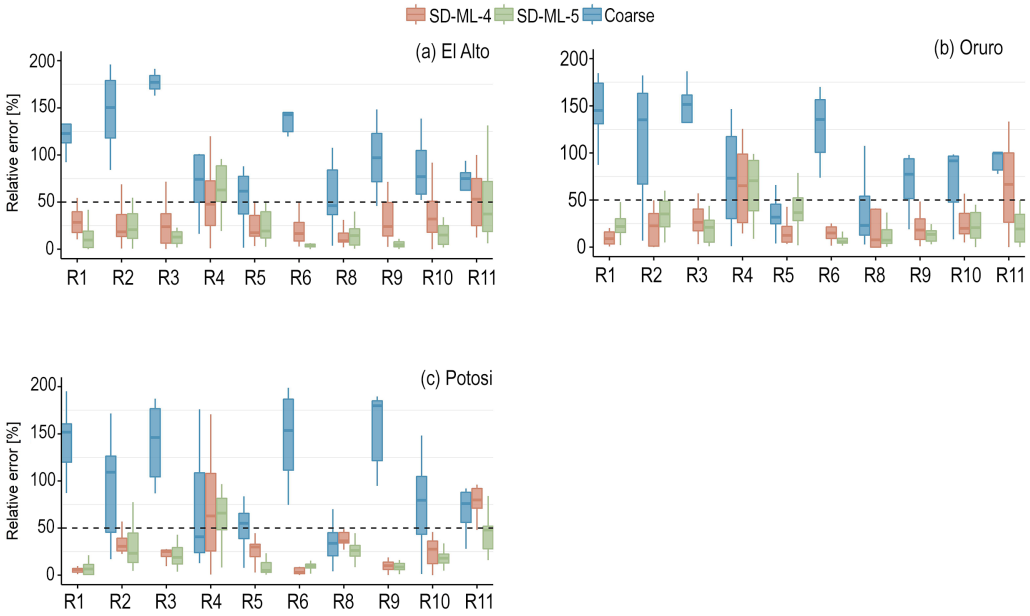

Figure 2. Relative errors in the highlands. stations are presented. The RIs obtained from the downscaled results of both SDMs are compared against the observations in 1961–1980. Moreover, the relative errors of the RIs derived from the coarse-scale values (GCM raw outputs) are also presented. The *X*-axis shows the different research indicators except R7 (maximum daily precipitation of a 30-year return period). The *Y*-axis represents the relative error in percentage.

Regarding the intensities of high extremes (R8), the GCMs reasonably captured the events, and the added value from the SDMs was seen only at El Alto and Oruro stations. For the case of high extreme event occurrences (R9 and R10), the methodologies corrected the values to less than 25% in most cases. SD-ML-5 seemed to outperform SD-ML-4 in correcting the occurrence of the highest events. As a summary, the relative errors of the downscaled results (medians) in all research indicators except R4 (winter precipitation) and R11 (annual count of days with precipitation greater than 30 mm) were less than 50%. Since most of the time, the GCMs contain errors larger than 50%, this is clear evidence of added value (good skill) from both methodologies.

3.1.2. The Andean Slopes

Figure 3 shows the relative errors in the stations of the Andean slopes. Again, similar patterns are seen in the relative errors of the coarse scale (raw GCM outputs), except for Cochabamba, in which the relative errors were larger than 200% for R2, R3, R4, and R6. In the mentioned indicators, the correction of the SDMs brought the indicators to less than 50% of relative error except for R4 (winter precipitation). However, despite the large relative error in R4, the added value of the methodologies was clear. Tarija station showed slightly different patterns, with a larger relative error and a larger interquartile range (more variability). Compared to Cochabamba and Sucre stations (where in most cases, the relative errors were below 25%), many indicators showed relative errors larger than 50%. The zone stations generally showed small relative errors (less than 50%) in R5 and R8, with smaller variability (smaller interquartile range) compared to the raw outputs except for SD-ML-5 for R8 in Tarija. This is important to emphasize since R5 and R8 denote the maximum duration of dry spells and the daily precipitation intensity for a 10-year return period, respectively, which were the most representative indicators for droughts and floods in this work.

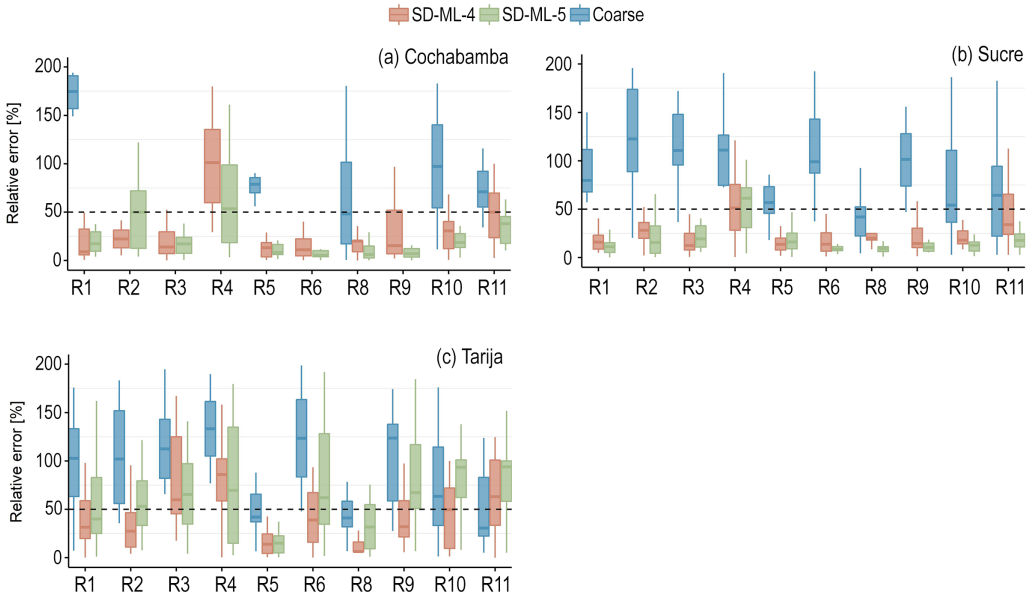

Figure 3. Relative errors in the Andean slopes. The RIs obtained from the downscaled results of both SDMs are compared against the observations in the period 1961–1980. Moreover, the relative errors of the RIs derived from the coarse-scale values (GCM raw outputs) are also presented. The *X*-axis shows the different research indicators except R7 (maximum daily precipitation of a 30-year return period). The *Y*-axis represents the relative error in percentage.

3.1.3. The Amazon Lowlands

The GCMs generally showed good skill in this zone (Figure 4). The majority of the relative errors for the indicators were below 50%. Hence, the added value from the SDMs was more difficult to investigate, and sometimes there was none (raw GCM data had a similar skill or was a better predictor). However, looking at Figure 4 in detail, one can notice that the SDMs performed well in R8 by reducing the relative error of the GCMs to less than 25%. For the mentioned indicator, SD-ML-4 showed a better downscaling in Guayaramerin, Rurrenabaque, Trinidad, and Trompillo, and SD-ML-5 in Cobija. Regarding winter precipitation (R4), the results showed poor skill (no added value) in Cobija, Rurrenabaque, and Guayaramerin, while in Trinidad and Trompillo, SD-ML-4 obtained reliable downscaled results with a median relative error of around 25%. Except for Cobija, SD-ML-4 outperformed SD-ML-5 in R5 (maximum duration of dry spells). Interestingly, in Cobija, the opposite happened in R8 (10-year return period precipitation). In all cases of high precipitation occurrences (R9, R10, and R11), both methodologies reduced the median relative error to less than 50%.

3.1.4. The Chaco Lowlands

The Chaco lowlands presented an unclear pattern for the zone (Figure 5). For instance, the GCMs in Yacuiba seemed to have better skills than those in Camiri. Moreover, the added value of the methodologies (reduction in the coarse-scale relative error) seemed clearer in Camiri than in Yacuiba. In fact, there were large coarse-scale relative error reductions in Camiri (in many cases, even the IQR was below 25% of relative error). However, regarding the more extreme events, the added value was only evident in Yacuiba for R5 with SD-ML-5 and R8 with SD-ML-4. In the occurrence of high precipitation events, both methodologies showed added value in Camiri. R2 (spring precipitation) was the indicator with the largest coarse-scale relative error at both stations in the zone. For this case, SD-ML-4 especially showed added value.

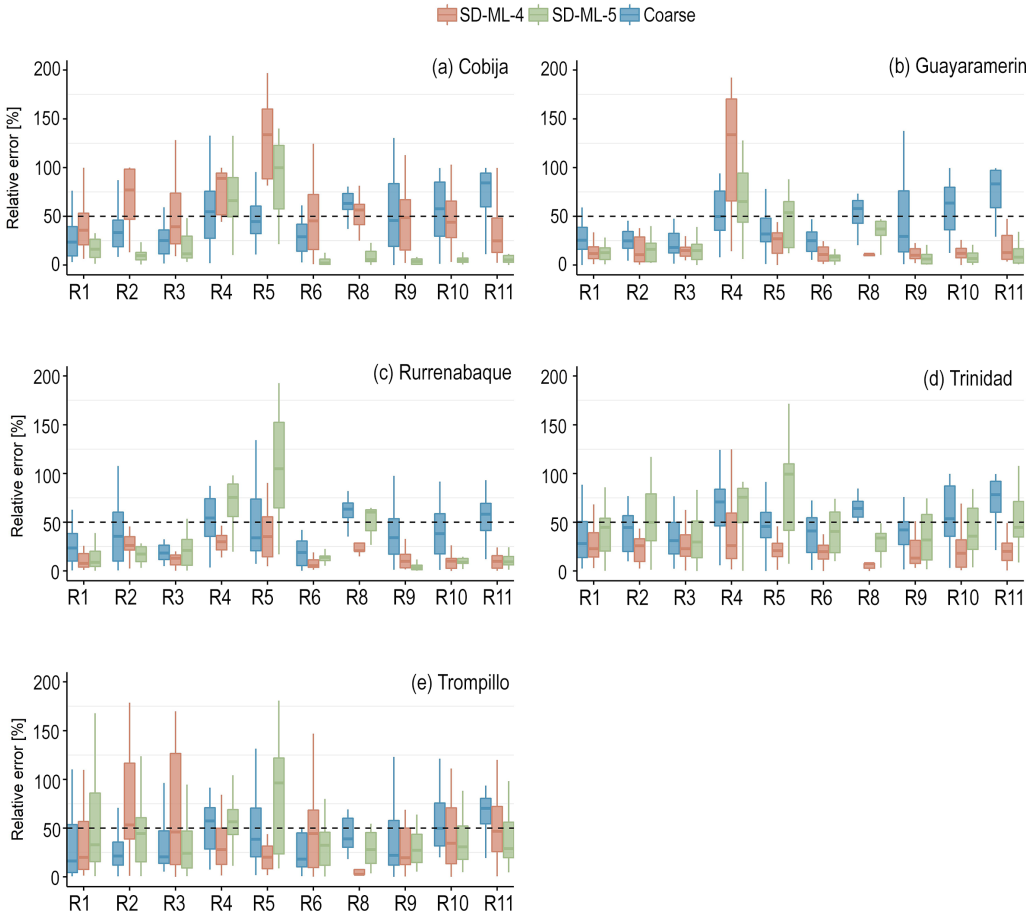

Figure 4. Relative errors in the Amazon lowlands. The RIs obtained from the downscaled results of both SDMs are compared against the observations in 1961–1980. Moreover, the relative errors of the RIs derived from the coarse-scale values (GCM raw outputs) are also presented. The *X*-axis shows the different research indicators except R7 (maximum daily precipitation of a 30-year return period). The *Y*-axis represents the relative error in percentage.

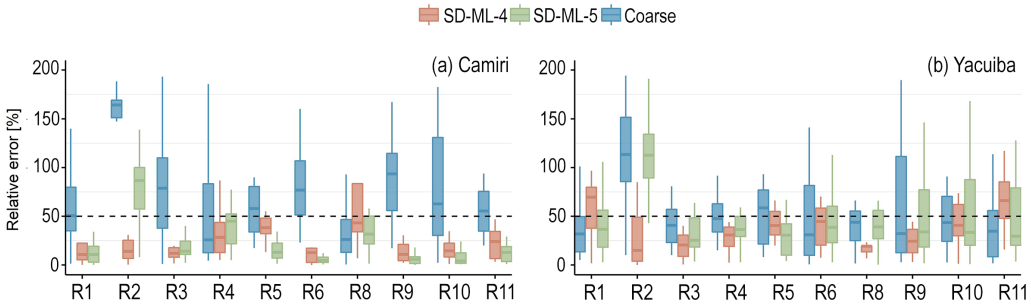

Figure 5. Relative errors in the Chaco lowlands. The RIs obtained from the downscaled results of both SDMs are compared against the observations in 1961–1980. Moreover, the relative errors of the RIs derived from the coarse-scale values (GCM raw outputs) are also presented. The *X*-axis shows the different research indicators except R7 (maximum daily precipitation of a 30-year return period). The *Y*-axis represents the relative error in percentage.

3.2. Uncertainty Contribution from the SDMs

In the highlands, the uncertainty share of the SDMs was dominant (Figure 6). The contribution from the GCMs rose in Oruro, especially for R10 and R11 (indicators of occurrences of high extreme events) to about 20.4% and 41.8%, respectively, but the contribution remained small compared to the SDMs. Moreover, the future scenarios were the second largest contributors.

The Andean slopes, especially the Sucre and Tarija stations, showed a similar pattern to the previous zone (Figure 7). One could see a notable increase in the GCMs' uncertainty share for Cochabamba station, up to 80.8% in R1. Unlike Sucre and Tarija, Cochabamba showed a large increase in R7–R9, which are indicators of extreme intensities. It is interesting to notice that the increase in the GCMs' uncertainty share was attached to the high precipitation intensities, because one would expect the highest contribution of the SDMs to be where large corrections have been made. Hence, in Sucre and Tarija, the SDMs' corrections in high precipitation intensities seemed larger than in Cochabamba. Apart from the mentioned indicators, the highest contributor to the uncertainties in the zone seemed to be the SDMs. Another common feature of the stations was that the R3 indicator had a large GCM´s share. This might be due to the poor Autumn precipitation representation of the GCMs in the zone.

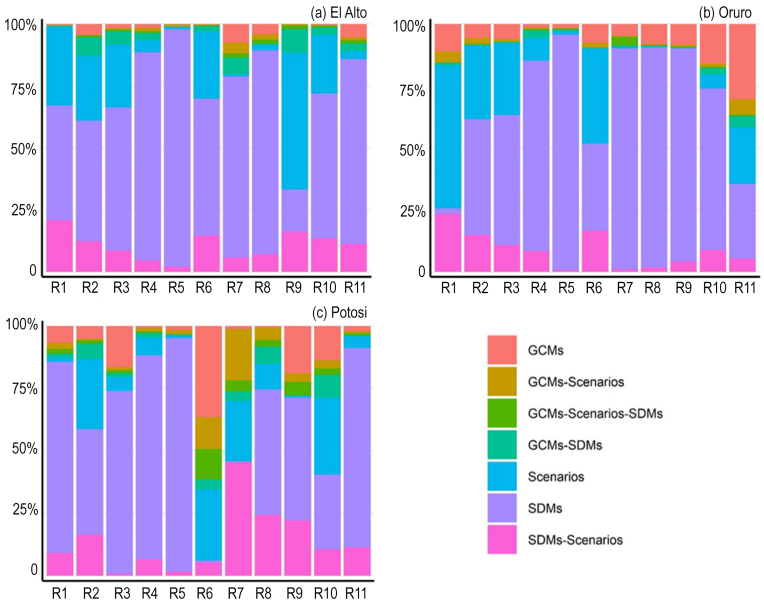

Figure 6. Uncertainty contribution from the different sources in the highlands. Each color represents the individual contribution to the total variance by the GCMs, SDMs, SSPs (scenarios), and the different second- and third-term interactions. R1, R2, . . . , and R11 denote the research indicators (see Table 3).

Compared to the highlands and Andean slopes, the Amazon lowlands contained a heterogeneous pattern (Figure 8). Although the SDMs had the highest uncertainty share in most cases, there were important contributions from the GCMs. Moreover, in some locations and indicators, the GCMs took over (e.g., R7 in Trompillo). Note that in Trinidad, the uncertainty share of the GCM–SDM interaction took over in most cases. The change in the pattern of the uncertainty contribution in Trinidad must be elaborated further as this increase in the interaction´s share could mean that in that zone, the use of a certain SDM method can give large differences in the results.

Similar to the other regions, the uncertainty share of the SDMs in the Chaco lowlands was dominant (Figure 9); however, there was a consistent increase in the share of the future scenarios. Note that in the indicators of high extremes intensities (R7 and R8), the single contribution (not total) of only the SDMs was not necessarily the largest. Moreover, in Yacuiba, with the 10-year and 30-year return period precipitation (R8 and R7), the SDMs were close in share (76.1% and 72.4%). Hence, the uncertainty contribution from the SDMs in high extreme precipitation events was evident in this area.

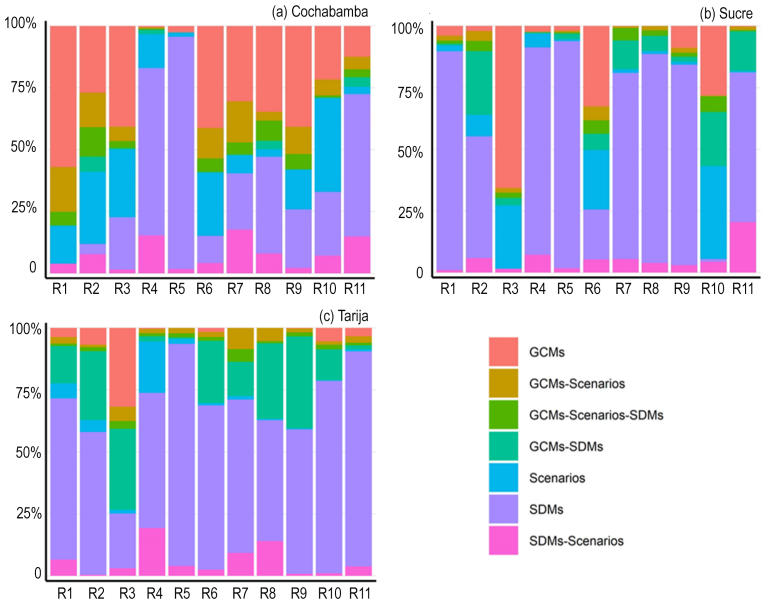

Figure 7. Uncertainty contribution from the different sources in the Andean slopes. Each color represents the individual contribution to the total variance by the GCMs, SDMs, SSPs (scenarios), and the different second- and third-term interactions. R1, R2, . . . , and R11 denote the research indicators (see Table 3).

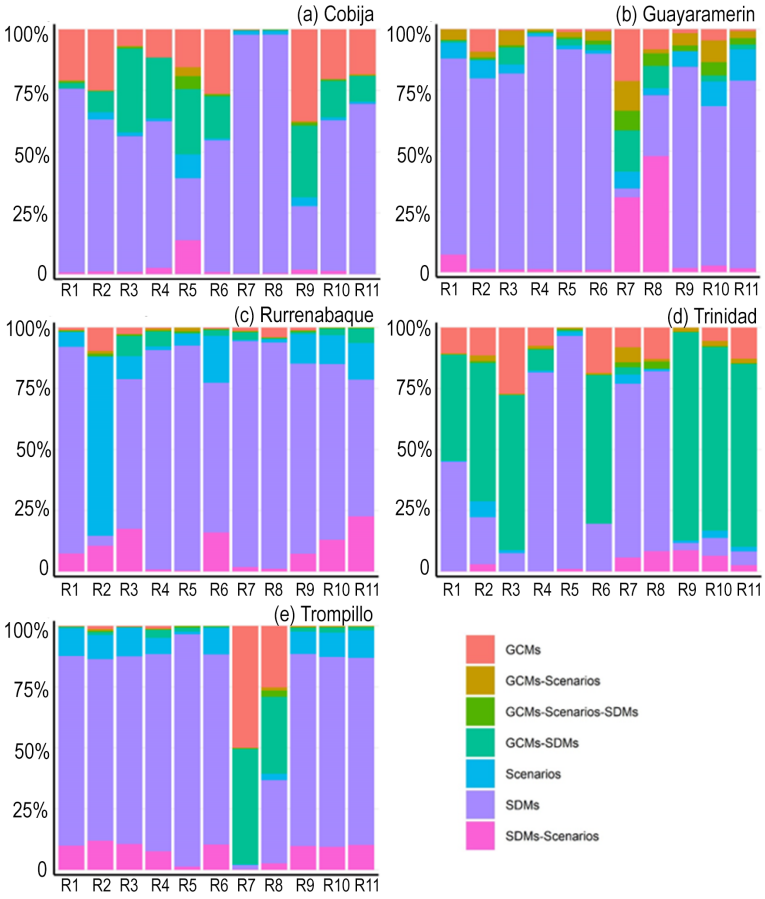

Figure 8. Uncertainty contribution from the different sources in the Amazon lowlands. Each color represents the individual contribution to the total variance by the GCMs, SDMs, SSPs (scenarios), and the different second- and third-term interactions. R1, R2, . . . , and R11 denote the research indicators (see Table 3).

3.3. Projections

For each future scenario (SSP1-2.6, SSP2-4.5, SSP3-7.0, and SSP5-8.5), tables with summaries from the downscaled results of the SDMs used in this work, random forest (SD-ML-4) and support vector machine (SD-ML-5), are presented. The projections are given in terms of change factors. Note that not all changes were reliable. First, the added value of the SDMs (skill) needed to be adequate. Secondly, the SDMs had to agree on the direction of change. Finally, the change had to be significant. This work presents the changes for the future scenarios SSP1-2.6 and SSP5-8.5 as the low and high scenarios, respectively (Tables 4 and 5). The other scenarios (SSP2-4.5 and SSP3-7.0) can be found in the Supplementary Materials.

The future scenario SSP1-2.6 was less perturbed regarding greenhouse gas emissions (i.e., most similar to historical conditions). More generalized results were observed by considering stations in the same zone. Regarding the projections for low extremes (R5), El Alto was projected to decrease by 32%, while the other stations in the highlands zone showed no significant change. On the Andean slopes, Cochabamba was projected to decrease by 37% and Tarija with no significant change. Guayaramerin, Trinidad, and Trompillo were projected to experience no significant changes in the Amazon lowlands, while Cobija and Rurrenabaque presented unreliable changes. On the Chaco lowlands, a 22% and 30% decrease was projected for Camiri and Yacuiba, respectively.

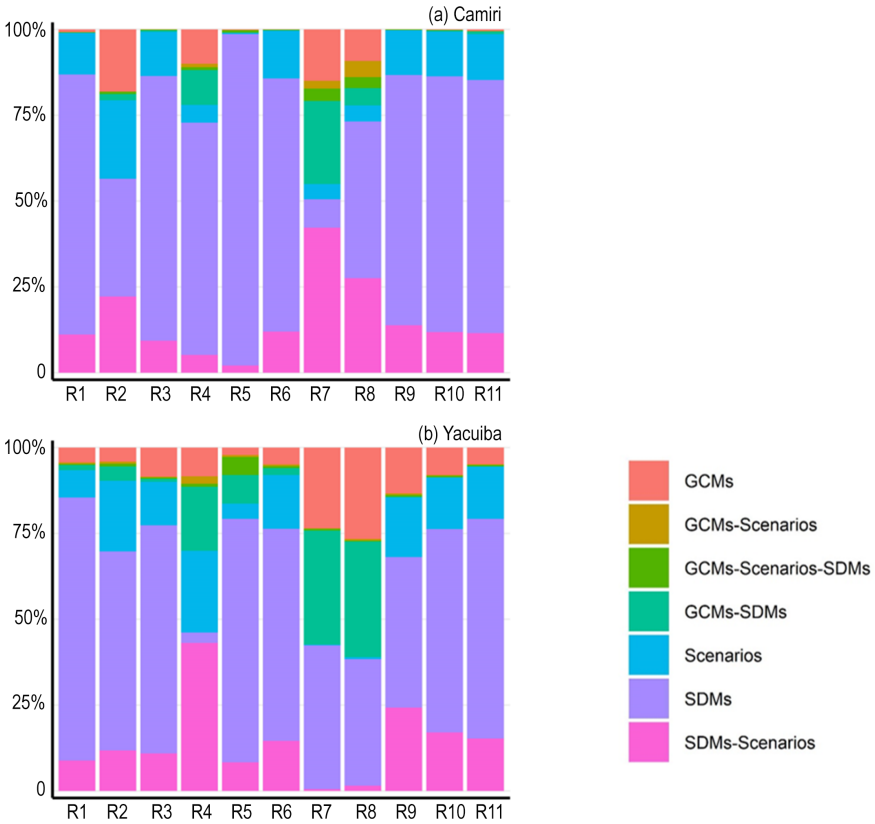

Figure 9. Uncertaintycontribution from the different sources in the Chaco lowlands. Each color represents the individual contribution to the total variance by the GCMs, SDMs, SSPs (scenarios), and the different second- and third-term interactions. R1, R2, . . . , and R11 denote the research indicators (see Table 3).

Table 4. Change factors for the SSP1-2.6 scenario. Change factors smaller than one denote decreases while larger increases. NCCS denotes no significant change; NR denotes unreliable projections. The CCS shown in the table is the average of the methodologies.

Future Scenario SSP1-2.6											
Station	**R1**	**R2**	**R3**	**R4**	**R5**	**R6**	**R7**	**R8**	**R9**	**R10**	**R11**
El Alto	NCCS	NCCS	1.25	NR	0.68	1.12	0.76	NCCS	1.06	1.63	0.74
Oruro	1.1	0.74	1.26	NR	NCCS	1.12	NCCS	NCCS	NR	NR	NR
Potosi	1.09	0.79	NR	NR	NCCS	1.05	NR	NR	1.08	1.33	NR
Cochabamba	1.06	1.33	NR	NR	0.63	1.15	NCCS	NCCS	NR	1.47	1.38
Sucre	NR	0.77	NCCS	NR	NR	NR	NCCS	NR	NR	1.2	1.25
Tarija	1.35	NR	1.89	NR	NCCS	1.51	0.79	NCCS	1.57	1.64	NR
Cobija	1.15	NCCS	NCCS	NR	NR	NCCS	0.66	NR	NCCS	NCCS	NR
Guayaramerin	NCCS	NR	1.28	NR	NCCS	NR	0.65	NR	1.14	1.19	1.3
Rurrenabaque	NR	1.18	0.78	0.74	NR	0.92	0.64	0.7	NR	NR	NR
Trinidad	NR	0.77	NR	1.54	NCCS	0.92	0.54	0.77	0.86	0.86	NCCS
Trompillo	NR	NR	NR	1.65	NCCS	NR	NCCS	NCCS	NR	1.51	1.82
Camiri	NR	1.31	NR	NR	0.78	1.18	NR	NR	NR	1.25	1.3
Yacuiba	NR	1.39	1.32	NCCS	0.7	NR	NCCS	1.19	NR	NR	NR

Table 5. Change factors for the SSP5-8.5 scenario. Change factors smaller than one denote decreases while larger increases. NCCS denotes no significant change; NR denotes unreliable projections. The CCS shown in the table is the average of the methodologies.

Future Scenario SSP5-8.5											
Station	**R1**	**R2**	**R3**	**R4**	**R5**	**R6**	**R7**	**R8**	**R9**	**R10**	**R11**
El Alto	1.42	NR	1.88	NR	0.68	1.59	0.76	0.82	1.47	NR	NR
Oruro	1.6	NR	2.07	NR	0.55	1.6	0.7	NR	NR	NR	NR
Potosi	NR	NR	1.25	NR	NR	1.08	NR	NR	NR	1.49	NR
Cochabamba	1.14	1.47	1.32	NR	0.61	1.31	0.83	NR	1.17	2.36	NR
Sucre	NR	0.84	1.13	NR	NR	1.08	NCCS	NR	NR	1.28	NR
Tarija	NR	1.54	2.1	NR	NR	1.5	0.79	NR	1.62	1.49	NR
Cobija	NR	0.82	1.09	NR	NR	0.94	NCCS	NCCS	0.9	NCCS	0.7
Guayaramerin	NCCS	NR	1.3	NR	NCCS	NR	0.65	0.77	NR	1.24	1.47
Rurrenabaque	0.65	0.83	0.53	0.66	NR	0.69	NCCS	NCCS	0.73	0.69	0.74
Trinidad	NR	0.72	NR	1.47	NCCS	0.86	NCCS	0.74	0.88	0.83	NCCS
Trompillo	NR	NR	NR	NR	NCCS	NR	NCCS	NCCS	NR	2.33	NR
Camiri	1.84	1.76	2.07	NR	NCCS	1.9	NR	NR	NR	2.17	2.89
Yacuiba	NR	2.45	1.89	NR	0.69	NR	NCCS	1.13	NR	NR	NR

The projections for high extreme intensities (R7 and R8) in the highlands generally showed no significant or unreliable changes. Only El Alto showed a decrease of about 24% in R7. The Andean slopes showed a similar situation except for Tarija, which was projected to have a 21% decrease in R7. More clear changes could be found in the Amazon lowlands. For R7, 34%, 35%, 36%, and 46% decreases were projected for Cobija, Guayaramerin, Rurrenabaque, and Trinidad, respectively. For R8, 30% and 23% decreases were projected in Rurrenabaque and Trinidad, respectively.

The high extreme precipitation occurrences (R9, R10, and R11) had more significant changes than the intensities. El Alto and Potosi project increased to 63% and 33% in the highlands, respectively. In the Andean slopes, increases of up to 47%, 25%, and 64% were projected for Cochabamba, Sucre, and Tarija, respectively. In the Amazon lowlands, increases of up to 30% and 82% were projected in Guayaramerin and Trompillo, respectively. Also, a decrease of 14% for R9 and R10 was noted in Trinidad. Only Camiri projected an increase (up to 30%) in the Chaco lowlands.

The changes in annual rainfall (R6) had a clear pattern in each zone. The highlands, the Andean slopes, and the Chaco lowlands had increases of 12%, 12%, 5%, 15%, 51%, and 18% in El Alto, Oruro, Potosi, Cochabamba, Tarija, and Camiri, respectively. The decreases

were projected in the Amazon lowlands, with 8% and 8% in Rurrenabaque and Trinidad, respectively. Moreover, Cobija projected no change in R6.

The future scenario SSP5-8.5 had the same pattern (direction of change) with more pronounced changes in general. Moreover, the SSP5-8.5 scenario had the highest forcing of all future scenarios in this work; hence, it was regarded as the high-end scenario. In the low extremes (R5), decreases were projected in all zones, with 32%, 45%, 39%, and 31% in El Alto, Oruro, Cochabamba, and Yacuiba, respectively.

In the high extreme intensities, decreases were projected in the highlands, Andean slopes, and Amazon lowlands (up to 24, 30%, 17%, 21%, 35%, and 26% in El Alto, Oruro, Cochabamba, Tarija, Guayaramerin, and Trinidad), with increases in the Chaco lowlands (13% in Yacuiba). For the case of the frequency of high extremes, increases were projected in all zones except the Amazon lowlands. The significant increases found were up to 47%, 49%, 17% 28%, and 62% in El Alto, Potosi, Cochabamba, Sucre, and Tarija, respectively. For the Amazon lowlands, there was no pattern since decreases (Cobija, Rurrenabaque, and Trinidad) and increases (Guayaramerin and Trompillo) were found.

Similar to the previous future scenario, the annual rainfall changes (R6) contained a strong spatial pattern. The highlands, Andean slopes, and Chaco lowlands were projected to have increases of 59%, 60%, 8%, 31%, 8%, 50%, and 90% in El Alto, Oruro, Potosi, Cochabamba, Sucre, Tarija, and Camiri, respectively. The Amazon lowlands might face a decrease in annual rainfall by about 6%, 31%, and 14% in Cobija, Rurrenabaque, and Trinidad.

4. Discussion

4.1. Skill and Uncertainty

It is interesting that, to some extent, the behavior of the SDMs was related to the zone in which they were applied. This happened because the downscaling methods are only as effective as the data they receive; if crucial information is missing at either large or local scales, the results cannot meaningfully improve our understanding of precipitation dynamics. In essence, these methods do not generate new insights; they merely leverage existing data to reveal hidden non-linear relationships. In other words, the skill dependency on different locations is expected.

4.1.1. Highlands

There was no confidence in the projections of winter precipitation according to the relative errors. This happened because the winter precipitation is entirely in the dry season. The dry season in the Andean region is characterized by almost no rain [34,35]. Hence, errors in small precipitation amounts are highly probable. Since the wrong estimations in low precipitation amounts can be very high due to the low values, some artifacts tend to appear. For instance, let us assume the total rainfall for a random month in the winter season is around 2 mm, and the estimations from a modeled source are around 11 mm; the relative error is 450%. This example might seem implausible at first sight; however, one must notice that GCMs tend to have a wet bias in the Andean region [36]. This wet bias in the dry season could easily introduce a difference similar to the example presented, causing large errors in the estimations and masking the added value of the methodologies.

Another feature common in the stations of the highlands zone was that the SDMs were the dominant source of uncertainty. This feature seems common in downscaling studies in many locations (e.g., [37]). There were some increases in the GCMs' contribution in the Oruro station; however, even with the highest increases (R10 and R11, see Section 3.2), the GCMs' uncertainty share remained small compared to the SDMs. Since the main source of uncertainties in the studies for the highlands zone is dominated by the SDMs, one has to ensure the validity of the SDMs used in the study to avoid unreliable projections.

4.1.2. Andean Slopes

In general, the SDMs showed added value (reduction in the relative error of the coarse scale) in the zone, which was usually true for both methodologies. The exception was Tarija, in which SD-ML-4 better downscaled the intensities and occurrences of high extremes. The large relative errors in the coarse scale (e.g., Cochabamba station) and the good improvements shown by both methodologies made the SDMs important in that zone for local projections.

A feature common in all the stations in the zone was the dominant SDMs' uncertainty share except for Cochabamba. It seemed strange because Sucre and Tarija Stations are located in places with large similarities in topography and climate compared to Cochabamba. By looking at Figure 3, one can argue that since the coarse scale was performing better in Cochabamba, the SDMs made smaller corrections. As a consequence, the differences on the corrected values were not too large. However, the better GCMs' performances in Cochabamba remains unclear and should be studied in more detail.

The large reduction in relative errors that the SDMs achieved in the zone and the reduction in the SDMs' uncertainty share in Cochabamba make the studied SDMs good candidates for a local analysis of the Andean slopes.

4.1.3. Amazon Lowlands

The Amazon lowlands are characterized by a more humid climate compared to the Chaco lowlands, even though they are close and have similar altitudinal gradients [22]. According to the relative errors, a general feature of the zone was that R4 projections (winter precipitation) might only be reliable in Trinidad and Trompillo and with SD-ML-4. Another clear feature was that the impact assessment of droughts might be better assessed with SD-ML-4 at all stations but Cobija due to the results for R5 (maximum duration of dry spells). On the other side of extremes, both methodologies might adequately describe the local series for the impacts of floods (intensity and occurrence). Note that in Cobija, SD-ML-5 appeared to be more reliable according to the relative error estimation of high extremes' indicators (R7, R8, R9, R10 and R11).

The uncertainty share of the GCMs became more important in that zone. The share of GCM-SDM interaction seemed to increase, e.g., Trinidad station. A similar feature was found for other regions as well (e.g., [38]). Interestingly, the GCMs' skill in that zone was also better compared to the highlands and the Andean slopes. It seems that when the GCMs' skill is good, the variability in the coarse-scale values (GCMs) can have an important contribution to the outcomes.

4.1.4. Chaco Lowlands

The results for the Amazon Chaco zone showed that both methodologies might add value to the GCMs' outputs while assessing droughts. However, SD-ML-5 outperformed SD-ML-4 on this matter as the performance was better in R5. For assessing the intensities of high extremes in the zone, only SD-ML-4 showed adequate results for Yacuiba. However, for the case of the occurrences of high extremes, both methodologies showed added value in Camiri while none in Yacuiba. Similar to other zones in the study (highlands and Andean slopes), R4 (winter precipitation) showed no added value, probably for the same reason as in the highlands and the Andean slopes.

The SDMs were the dominant source of uncertainty. Interestingly, the coarse-scale relative error in R8 in Camiri was low, and no added value was seen from the SDMs. At the same time, the SDM' share was reduced, and the GCMs' share seemed to increase. As stated for the Amazon lowlands, it seemed that in some situations, the coarse-scale climate might have important impacts in the variability of the results.

4.2. Assumptions of the SDMs

The reference period (historical) contained relationships calibrated from 1981 to 2010, and the relative errors were calculated with the downscaled results from 1961 to 1980.

Thus, (i) the time invariance of the architectures could be investigated. Moreover, since the historical period (1981–2010) might have different forcings than 1961–1980, the assumption that (ii) the calibrated relationships work under different forcing conditions might be partially assessed. Bias correction was embedded in the downscaling procedures; hence, the time invariance of the bias followed the conclusions of (i) and (ii). The methodologies based their corrections on the assumption that (iii) the GCMs were accurate enough and the errors appeared only due to the low spatial resolution. Therefore, the magnitudes of the coarse-scale relative errors might give information on this matter. Lastly, the machine learning methodologies assumed (iv) the wet/dry day frequency correction and dry spell duration accuracy. The relative error results for indicator R5 (maximum duration of dry spells) were considered for this. In this way, one could investigate whether the wet/dry day frequency correction was adequate and suitable for tackling dry spell duration.

Time invariance of the architecture (i): By analyzing the relative errors (skill), one can see that the time invariance of the architectures was highly dependent on the location rather than the methodologies. Nevertheless, the methodologies generally seemed to work fine outside the calibration period. The latter can be seen because the added value of both methodologies was clear in many cases, and the 20-year period in which the relative errors were defined (1961–1980) was completely independent from the 30-year period (1981–2010) in which the relationships were obtained.

Relationships work under different forcing conditions (ii): Evidence shows that the climate after 2000 is already perturbed by a higher increased warming trend [39]. Hence, the calibration period (1981–2010) might have slightly different forcings compared to the period 1961–1980. A small relative error might be an indication that the relationships are robust enough to be used under different forcing conditions. The results showed that the latter was highly related to the zone because the added value (skill) at the stations in the lowlands was less clear.

Accurate predictors (iii): In the highlands and Andean slopes, this assumption seemed to be weak, especially for Cochabamba, in which the GCMs performed poorly. The reason might be the topography and precipitation complexity of the zones. In the lowlands, this assumption seemed to hold. While many reasons might cause this, the clearest one (since this assumption on the highlands and Andean slopes was not robust) is the topography. The lowlands contain lower complexity in the topography as the region is generally flat, and processes like orography rainfall could not happen. A similar feature can be seen in Rivera and Arnould [36], who showed that the CMIP6 GCMs tended to have less skill in the Andean mountainous regions with low precipitation rates, while the skill seemed better closer to the zones with low altitudes.

Accuracy of the wet/dry day frequency correction and dry spell duration (iv): Most of the time, the results regarding the maximum duration of dry spells (R5) were quite robust. This means that the methodologies used in this work could cope with the dry/wet day frequency correction and the correction of the spell duration. The latter is essential to test as Boé et al. [40] showed that the dry/wet day frequency correction did not necessarily imply accuracy in the duration of dry spells. However, the wet spells were not tested in this work; hence, the finding is only valid for the dry spell duration. The wet/dry day frequency and their duration are highly attached to the occurrence of droughts. Therefore, the methodologies presented here seem to be valid for such studies. Additionally, note that the dry frequency correction in SD-ML-5 (which is, in principle, a hybrid machine learning–bias correction procedure) did not assume a wet bias as other studies with bias correction procedures (e.g., [41]). Finally, notice that the SDMs did not show added value in the winter precipitation (dry season). Therefore, the use of these methodologies for drought studies needs to be studied further.

4.3. Expected Projections for the Region

Since reliable projections need to be investigated, one must establish whether the projected change is uncertain (unreliable), significant, or non-significant. A significant change

happens when the projection agrees with the direction of change in both methodologies (SD-ML-4 and SD-ML-5), and one of the SDMs or both show a significant change. An uncertain change appears when both SDMs project significant changes and disagree on the change's direction. When the SDMs do not project significant changes, the projection is considered non-significant. Note that the relative errors also drive the discussion. When the methodology has poor skill on a specific research indicator (no added value according to the relative errors), the projections are considered unreliable. Finally, the future scenarios SSP1-2.6 and SSP5-8.5 were considered the most and the least optimistic scenarios (lower and high-end scenarios), respectively.

As a general feature for all future scenarios in the highlands, the projections for the winter precipitation could be regarded as unreliable. According to SSP1-2.6, the zone could face a decline in the dry spell duration due to the decrease shown by El Alto. This feature was more pronounced in the SSP5-8.5 scenario, as more stations (El Alto and Oruro) showed the reduction. On the one hand, the stations had a disagreement in the SSP1-2.6 projections for the intensities of high precipitation events, but the dominant feature was that no significant change could happen. However, an increase in the high precipitation events' frequency was noted as dominant in that zone. On the other hand, scenario SSP5-8.5 had a clearer projected decrease in the intensities while the projected increase in the frequencies became less clear. Regarding the annual rainfall, the governing feature of SSP1-2.6 was the increased precipitation amounts (up to 12%). The scenario SSP5-8.5 had a similar pattern but with larger increases (up to 60%).

The projected increase in annual precipitation in the highlands is in disagreement with the ensemble mean in Meehl et al. [42] or the dynamically downscaled precipitation in Nuñez et al. [43]. However, one must notice that the mentioned studies contained old-generation models with different future scenarios. Moreover, neither study contained projections for local scale stations, a feature that might be causing the disagreements. Additionally, some studies noted that a future increase in annual rainfall in these Andes locations was possible [44]. Oppositely to Abadi et al. [45], the dry spell duration was projected to decrease in the highlands. However, that study analyzed Bolivia with five GCMs and the CMIP5 generation. The ensemble studied here was larger (20 GCMs) and belonged to the CMIP6 generation. Moreover, the present work performed an analysis on a local daily scale, a feature missing in the last mentioned study, which could be the cause of the disagreement.

In the Andean slopes, the future scenario SSP1-2.6 tended to project a higher frequency of high rainfall events (up to 64%). The SSP5-8.5 scenario showed a similar behavior but remained uncertain to what extent (larger or smaller projections) as there was no general feature. There was no zonal feature on the low extremes (R5). However, Cochabamba was projected to have a decrease in the dry spell duration in both future scenarios (SSP1-2.6 and SSP5-8.5). Regarding annual rainfall, the zone's dominant feature was the future increase. SSP1-2.6 projected an increase of up to 51% and SSP5-8.5 of up to 50%. Hence, the increase was similar for both future scenarios even though SSP5-8.5 was the high-end scenario.

In the Amazon lowlands, the projections for both future scenarios in the low extremes of the zone remained uncertain. Some stations projected no change, while others showed unreliable changes. The pattern was also unclear on the high precipitation events' frequency as some stations projected an increase (e.g., Guayaramerin) and others a decrease (e.g., Trinidad). Note that while the decreases were of the same order in both future scenarios, the increases tended to become larger in SSP5-8.5. A clearer trend (decrease) was found in the intensities of high precipitation events, which were of the same order for both future scenarios (up to 46% in SSP1-2.6). Finally, the zone's projected decrease in annual rainfall for all stations was noticeable and was more pronounced in SSP5-8 (up to 31%).

Some results in the Amazon lowlands agreed with Cabré et al. [46], while others disagreed (depending on the stations). Nevertheless, one must notice that the dynamical downscaled ensemble in the mentioned study was limited to one model, and the outputs depended on an old generation of models (CMIP3). Furthermore, the results in this work

are intended for the local level, while Cabré et al. [46] presented the projections at the regional level.

In the Chaco lowlands, the future scenarios projected a decrease in the dry spells' duration of a similar order. Regarding high extremes, there was a notable increase in frequency (Camiri) and intensity (Yacuiba). These increases seemed more pronounced for SSP5-8.5 in the frequency of the events. On cumulated precipitation amounts, an increase was noted for annual rainfall. This feature is in agreement with the Eastern Andean projections in Cabré et al. [46]) and Meehl et al. [42].

5. Conclusions

SD-ML-4 performed better than SD-ML-5 in many situations for downscaling GCMs, but SD-ML-5 excelled where SD-ML-4 did not add value. Both methods showed greater skill in the highlands and Andean slopes compared to the lowlands, where performance dropped, especially in the Amazon and Chaco regions. Errors related to topographical complexity were largely mitigated by the SDMs. Rather than seeking the best method, it was more effective to explore suitable ensembles for downscaling.

The stationary assumptions were valid for the highlands and Andean slopes, but uncertain for the lowlands. While the accurate predictors assumption was robust in the lowlands, it weakened in the highlands, particularly at the Cochabamba station due to its topographical complexity. The wet/dry day frequency correction and dry spell duration accuracy assumption generally held, with SD-ML-5 outperforming SD-ML-4.

Uncertainty mainly arose from SDMs, especially in the highlands and Andean slopes (except Cochabamba). In the Amazon and Chaco lowlands, GCMs contributed more to total uncertainty, though SDMs still dominated. Regarding high extreme rainfall, GCMs may become the primary source of uncertainty when downscaling does not enhance coarse-scale results.

All locations faced water availability issues in the dry season. Projections suggested only the Amazon lowlands may experience reduced annual rainfall, particularly under the SSP5-8.5 scenario. For dry spell duration, the stations with significant changes indicated decreases, but no reliable changes were observed in the Amazon lowlands. Increased frequency of high precipitation events was projected region-wide, except for Cobija, Rurrenabaque, and Trinidad. This poses challenges, as urban infrastructure may not cope with flooding, especially where high extreme intensity increases are projected. The increase in high intensities at Yacuiba came with uncertain high precipitation frequency projections, leaving the increased flood risk (compared to other locations) ambiguous.

Some limitations need to be acknowledged: (i) Not all the stations in Bolivia were used; a higher station density is needed for clearer patterns and robust results. (ii) Stations from other countries in the region (South America) need to be used to generalize and confirm the findings. (iii) GCMs have particular problems in the Andean valleys, probably due to the topographical complexity in the zone. The use of regional models might be better to represent the lost processes in the GCMs. (iv) The investigation that the relations remain the same under different forcing conditions is limited. Hence, a pseudo-reality study (e.g., [8,41]) might be interesting for more robust findings.

Supplementary Materials: The following supporting information can be downloaded at: https://www.mdpi.com/article/10.3390/w16213070/s1.

Author Contributions: Conceptualization S.M.P., P.W. and M.F.V.G.; formal analysis, S.M.P.; methodology, S.M.P., P.W. and M.F.V.G.; software, S.M.P.; supervision, P.W.; validation, S.M.P.; writing—original draft, S.M.P.; writing—review and editing, P.W. and M.F.V.G. All authors have read and agreed to the published version of the manuscript

Funding: This research did not receive any specific grant from funding agencies in the public, commercial, or not-for-profit sectors.

Data Availability Statement: CMIP6 GCM outputs are freely available at the ESGF website (https://esgf-data.dkrz.de, accessed on 1 February 2023). The meteorological datasets of the air-

ports were provided by the Bolivian National Services of Meteorology and Hydrology (SENAMHI), website: (https://senamhi.gob.bo/index.php/inicio, accessed on 1 March 2023).

Acknowledgments: We are grateful to the Bolivian National Services of Meteorology and Hydrology (SENAMHI) as their data were crucial to develop this work.

Conflicts of Interest: The authors declare that they have no conflicts of interest.

Abbreviations

The following abbreviations are used in this manuscript:

CCS	Climate change signal
CMIP6	Coupled Model Intercomparison Project Phase 6
ECMWF	European Centre for Medium-Range Weather Forecasts
ESD	Empirical statistical downscaling
ETCCDI	Expert Team on Climate Change Detection and Indices
GCM	Global climate model
MLT	Machine learning technique
MSL	Meters above Sea Level
NSWT	Nonhomogeneous stochastic weather typing
RF	Random forest
SDM	Statistical downscaling method
SENAMHI	Servicio Nacional de Hidrometeorología
S2NR	Signal-to-noise ratio
SVM	Support vector machines

References

1. Smithers, J.; Smit, B. Human adaptation to climatic variability and change. *Glob. Environ. Change* **1997**, *7*, 129–146. [CrossRef]
2. Phillips, S.; Wallis, K.; Lane, A. Quantifying the impacts of bushfire on populations of wild koalas (*Phascolarctos cinereus*): Insights from the 2019/20 fire season. *Ecol. Manag. Restor.* **2021**, *22*, 80–88. [CrossRef]
3. British Broadcasting Corporation. *Brazil Floods: Dozens Dead in Severe Minas Gerais Rainstorms*; British Broadcasting Corporation: London, UK, 2020.
4. Gonzales-Iwanciw, J.; Salamanca, L.; Condori, B.; Ontiveros, M. *Tras las Huellas del Cambio climáTico en Bolivia. Estado del Arte del Conocimiento Sobre Adaptación al Cambio climáTico*; Technical Report; PNUD: La Paz, Bolivia, 2011.
5. World Bank. *Adaptation to Climate Change—Vulnerability Assessment and Economic Aspects: Plurinational State of Bolivia*; Technical Report; World Bank: Washington, DC, USA, 2010.
6. Cardona, O.; Carreño, M. Updating the Indicators of Disaster Risk and Risk Management for the Americas. *J. Integr. Disaster Risk Manag.* **2011**, *1*, 27–47. [CrossRef]
7. Knutti, R.; Sedláček, J. Robustness and uncertainties in the new CMIP5 climate model projections. *Nat. Clim. Change* **2013**, *3*, 369–373. [CrossRef]
8. Vrac, M.; Stein, M.L.; Hayhoe, K.; Liang, X.Z. A general method for validating statistical downscaling methods under future climate change. *Geophys. Res. Lett.* **2007**, *34*, L18701. [CrossRef]
9. Benestad, R.; Sillmann, J.; Thorarinsdottir, T.L.; Guttorp, P.; Mesquita, M.d.S.; Tye, M.R.; Uotila, P.; Maule, C.F.; Thejll, P.; Drews, M.; et al. New vigour involving statisticians to overcome ensemble fatigue. *Nat. Clim. Change* **2017**, *7*, 697–703. [CrossRef]
10. Maraun, D.; Wetterhall, F.; Ireson, A.M.; Chandler, R.E.; Kendon, E.J.; Widmann, M.; Brienen, S.; Rust, H.W.; Sauter, T.; Themeßl, M.; et al. Precipitation downscaling under climate change: Recent developments to bridge the gap between dynamical models and the end user. *Rev. Geophys.* **2010**, *48*, RG3003. [CrossRef]
11. Chadwick, R.; Coppola, E.; Giorgi, F. An artificial neural network technique for downscaling GCM outputs to RCM spatial scale. *Nonlinear Process. Geophys.* **2011**, *18*, 1013–1028. [CrossRef]
12. Das, J.; Nanduri, U.V. Assessment and evaluation of potential climate change impact on monsoon flows using machine learning technique over Wainganga River basin, India. *Hydrol. Sci. J.* **2018**, *63*, 1020–1046. [CrossRef]
13. Hewitson, B.; Crane, R. Climate downscaling: Techniques and application. *Clim. Res.* **1996**, *7*, 85–95. [CrossRef]
14. Jebeile, J.; Lam, V.; Räz, T. Understanding climate change with statistical downscaling and machine learning. *Synthese* **2021**, *199*, 1877–1897. [CrossRef]
15. Tripathi, S.; Srinivas, V.; Nanjundiah, R.S. Downscaling of precipitation for climate change scenarios: A support vector machine approach. *J. Hydrol.* **2006**, *330*, 621–640. [CrossRef]
16. Vu, M.T.; Aribarg, T.; Supratid, S.; Raghavan, S.V.; Liong, S.Y. Statistical downscaling rainfall using artificial neural network: Significantly wetter Bangkok? *Theor. Appl. Climatol.* **2016**, *126*, 453–467. [CrossRef]

17. Kühnlein, M.; Appelhans, T.; Thies, B.; Nauss, T. Improving the accuracy of rainfall rates from optical satellite sensors with machine learning—A random forests-based approach applied to MSG SEVIRI. *Remote. Sens. Environ.* **2014**, *141*, 129–143. [CrossRef]
18. Salimi, A.H.; Masoompour Samakosh, J.; Sharifi, E.; Hassanvand, M.R.; Noori, A.; von Rautenkranz, H. Optimized Artificial Neural Networks-Based Methods for Statistical Downscaling of Gridded Precipitation Data. *Water* **2019**, *11*, 1653. [CrossRef]
19. Wilby, R.L.; Dessai, S. Robust adaptation to climate change. *Weather* **2010**, *65*, 180–185. [CrossRef]
20. Dixon, K.W.; Lanzante, J.R.; Nath, M.J.; Hayhoe, K.; Stoner, A.; Radhakrishnan, A.; Balaji, V.; Gaitán, C.F. Evaluating the stationarity assumption in statistically downscaled climate projections: Is past performance an indicator of future results? *Clim. Change* **2016**, *135*, 395–408. [CrossRef]
21. Seiler, C.; Hutjes, R.W.A.; Kabat, P. Climate Variability and Trends in Bolivia. *J. Appl. Meteorol. Climatol.* **2013**, *52*, 130–146. [CrossRef]
22. Water, M.; Bolivia, E. (Eds.) *Balance Hídrico Superficial de Bolivia: Documento de Difusión*; Ministerio de Medio Ambiente y Agua: La Paz, Bolivia, 2016; OCLC: on1007678949.
23. Araya-Osses, D.; Casanueva, A.; Román-Figueroa, C.; Uribe, J.M.; Paneque, M. Climate change projections of temperature and precipitation in Chile based on statistical downscaling. *Clim. Dyn.* **2020**, *54*, 4309–4330. [CrossRef]
24. Breiman, L. Random Forests. *Kluwer Acad. Publ.* **2001**, *45*, 5–32.
25. Pedregosa, F.; Varoquaux, G.; Gramfort, A.; Michel, V.; Thirion, B.; Grisel, O.; Blondel, M.; Prettenhofer, P.; Weiss, R.; Dubourg, V.; et al. Scikit-learn: Machine Learning in Python. *J. Mach. Learn. Res.* **2011**, *12*, 2825–2830.
26. Bjerre, E.; Fienen, M.N.; Schneider, R.; Koch, J.; Højberg, A.L. Assessing spatial transferability of a random forest metamodel for predicting drainage fraction. *J. Hydrol.* **2022**, *612*, 128177. [CrossRef]
27. Karatzoglou, A.; Smola, A.; Hornik, K.; Zeileis, A. kernlab—An S4 Package for Kernel Methods in R. *J. Stat. Softw.* **2004**, *11*, 1–20. [CrossRef]
28. Haykin, S. *Neural Networks: A Comprehensive Foundation*, 9th indian reprint ed.; Pearson Education: Delhi, India, 2005.
29. Räty, O.; Räisänen, J.; Ylhäisi, J.S. Evaluation of delta change and bias correction methods for future daily precipitation: Intermodel cross-validation using ENSEMBLES simulations. *Clim. Dyn.* **2014**, *42*, 2287–2303. [CrossRef]
30. Déqué, M.; Somot, S.; Sanchez-Gomez, E.; Goodess, C.M.; Jacob, D.; Lenderink, G.; Christensen, O.B. The spread amongst ENSEMBLES regional scenarios: Regional climate models, driving general circulation models and interannual variability. *Clim. Dyn.* **2012**, *38*, 951–964. [CrossRef]
31. Déqué, M.; Rowell, D.P.; Lüthi, D.; Giorgi, F.; Christensen, J.H.; Rockel, B.; Jacob, D.; Kjellström, E.; de Castro, M.; van den Hurk, B. An intercomparison of regional climate simulations for Europe: Assessing uncertainties in model projections. *Clim. Change* **2007**, *81*, 53–70. [CrossRef]
32. Hosseinzadehtalaei, P.; Tabari, H.; Willems, P. Precipitation intensity–duration–frequency curves for central Belgium with an ensemble of EURO-CORDEX simulations, and associated uncertainties. *Atmos. Res.* **2018**, *200*, 1–12. [CrossRef]
33. Tabari, H.; Hosseinzadehtalaei, P.; AghaKouchak, A.; Willems, P. Latitudinal heterogeneity and hotspots of uncertainty in projected extreme precipitation. *Environ. Res. Lett.* **2019**, *14*, 124032. [CrossRef]
34. Campozano, L.; Célleri, R.; Trachte, K.; Bendix, J.; Samaniego, E. Rainfall and Cloud Dynamics in the Andes: A Southern Ecuador Case Study. *Adv. Meteorol.* **2016**, *2016*, 3192765. [CrossRef]
35. Ruiz-Hernández, J.C.; Condom, T.; Ribstein, P.; Le Moine, N.; Espinoza, J.C.; Junquas, C.; Villacís, M.; Vera, A.; Muñoz, T.; Maisincho, L.; et al. Spatial variability of diurnal to seasonal cycles of precipitation from a high-altitude equatorial Andean valley to the Amazon Basin. *J. Hydrol. Reg. Stud.* **2021**, *38*, 100924. [CrossRef]
36. Rivera, J.A.; Arnould, G. Evaluation of the ability of CMIP6 models to simulate precipitation over Southwestern South America: Climatic features and long-term trends (1901–2014). *Atmos. Res.* **2020**, *241*, 104953. [CrossRef]
37. Mandal, S.; Breach, P.A.; Simonovic, S.P. Uncertainty in Precipitation Projection under Changing Climate Conditions: A Regional Case Study. *Am. J. Clim. Change* **2016**, *05*, 116–132. [CrossRef]
38. Lafaysse, M.; Hingray, B.; Mezghani, A.; Gailhard, J.; Terray, L. Internal variability and model uncertainty components in future hydrometeorological projections: The Alpine Durance basin. *Water Resour. Res.* **2014**, *50*, 3317–3341. [CrossRef]
39. O'Neill, B.C.; Tebaldi, C.; van Vuuren, D.P.; Eyring, V.; Friedlingstein, P.; Hurtt, G.; Knutti, R.; Kriegler, E.; Lamarque, J.-F.; Lowe, J.; et al. The Scenario Model Intercomparison Project (ScenarioMIP) for CMIP6. *Geosci. Model Dev.* **2016**, *9*, 3461–3482. [CrossRef]
40. Boé, J.; Terray, L.; Habets, F.; Martin, E. Statistical and dynamical downscaling of the Seine basin climate for hydro-meteorological studies. *Int. J. Climatol.* **2007**, *27*, 1643–1655. [CrossRef]
41. Mendoza Paz, S.; Willems, P. Uncovering the strengths and weaknesses of an ensemble of quantile mapping methods for downscaling precipitation change in Southern Africa. *J. Hydrol. Reg. Stud.* **2022**, *41*, 101104. [CrossRef]
42. Meehl, G.; Stocker, T.; Collins, W.; Friedlingstein, P.; Gaye, A.; Gregory, J.; Kitoh, A.; Knutti, R.; Murphy, J.; Noda, A.; et al. Global Climate Projections. In *Climate Change 2007: The Physical Science Basis. Contribution of Working Group I to the Fourth Assessment Report of the Intergovernmental Panel on Climate Change*; Solomon, S., Qin, D., Manning, M., Chen, Z., Marquis, M., Averyt, K.B., Tignor, M., Miller, H.L., Eds.; Cambridge University Press: Cambridge, UK; New York, NY, USA, 2007.
43. Nuñez, M.N.; Solman, S.A.; Cabré, M.F. Regional climate change experiments over southern South America. II: Climate change scenarios in the late twenty-first century. *Clim. Dyn.* **2009**, *32*, 1081–1095. [CrossRef]

44. Urrutia, R.; Vuille, M. Climate change projections for the tropical Andes using a regional climate model: Temperature and precipitation simulations for the end of the 21st century. *J. Geophys. Res.* **2009**, *114*, D02108. [CrossRef]
45. Abadi, A.M.; Oglesby, R.; Rowe, C.; Mawalagedara, R. Evaluation of GCMs historical simulations of monthly and seasonal climatology over Bolivia. *Clim. Dyn.* **2018**, *51*, 733–754. [CrossRef]
46. Cabré, M.F.; Solman, S.; Núñez, M. Regional climate change scenarios over southern South America for future climate (2080-2099) using the MM5 Model. Mean, interannual variability and uncertainties. *Atmósfera* **2016**, *29*, 35–60. [CrossRef]

Disclaimer/Publisher's Note: The statements, opinions and data contained in all publications are solely those of the individual author(s) and contributor(s) and not of MDPI and/or the editor(s). MDPI and/or the editor(s) disclaim responsibility for any injury to people or property resulting from any ideas, methods, instructions or products referred to in the content.